Chapter 4
Satellite Based Cloud Detection and Rainfall Estimation in the Upper Blue Nile Basin

Tom H.M. Rientjes, Alemseged T. Haile, Ambro S.M. Gieske, Ben H.P. Maathuis, and Emad Habib

Abstract In this study remote sensing for rainfall estimation is evaluated. For the Lake Tana basin in Ethiopia the diurnal cycle of rainfall is assessed using satellite observations at high temporal resolution and ground based observations. Also convective activity of a cloud system on the lake has been observed through satellite imagery and shows a potential to observe characteristics of a cloud that produced extreme rainfall intensity. These characteristics include the cloud area and a volume index as well as temporal evolution of distance and direction of the centroid of a cloud mass from a rain gauge at the Gurer Island in Lake Tana. In this work it is concluded that remote sensing can be very helpful in estimating rainfall, assessing the diurnal cycle and monitoring heavy rainfall producing clouds. The high potential of remote sensing observations is mainly because the observations are consistently available with spatially continuous coverage.

Keywords Satellite rainfall estimation · Diurnal cycle · Cloud tracking · Lake Tana

4.1 Introduction

Rainfall studies often are restricted by data availability. Estimation of rainfall is challenging in particular when rainfall largely varies over small time and space domains. Under such conditions, ground based rain gauge networks are commonly too sparse to satisfactorily capture the real world spatial distribution of rainfall properties such as rainfall intensity, duration and frequency. To overcome such limitation, the use of meteorological satellites is often advocated. Such satellites have applications in cloud detection and rainfall estimation. Examples of missions are the Tropical Rainfall Measuring Mission (TRMM) and the series of Meteosat satellites from which the Meteosat Second Generation (MSG-2) satellite is used in this study.

T.H.M. Rientjes (✉)
Department of Water Resources, Faculty of Geoinformation Science and Earth Observation (ITC), Twente University, 7500 AA Enschede, The Netherlands
e-mail: t.h.m.rientjes@utwente.nl

A.M. Melesse (ed.), *Nile River Basin*, DOI 10.1007/978-94-007-0689-7_4,

Meteorological satellites serve to detect rain producing clouds as well as to estimate rainfall over selected time-space domains. These satellites can be in orbit or can be geostationary. The first group overpasses a certain geographic area with a revisit time of ones or twice per day while the second group allows observations at frequency of $\geq$15 min. Orbital satellites such as TRMM observe a continuously changing geographic area while geostationary satellites such as MSG-2 observed the same area for the live time of the satellite. Earth orbiting satellites commonly fly at an altitude of hundreds of kilometers (e.g. 403 km for TRMM) while geostationary satellites commonly are positioned at high altitudes (e.g. 36,000 km for MSG-2 satellite).

In remote sensing based rainfall estimation, the most commonly utilized parts of the electromagnetic wave spectrum are the thermal infrared (TIR) and the microwave (MW) channels. These channels produce complementary information regarding rainfall that resulted in the development of combined TIR-MW based approaches. Currently, MW sensors are mounted only on orbiting satellites while TIR sensors are carried by orbiting as well as by geostationary satellites. It is noted that other channels such as the Visible (VIS) and the Water vapor (WV) channels are available as well but these are not used frequently despite that the channels have a potential to provide additional and complementary information about cloud characteristics (see, Lovejoy and Austin, 1979; Tsonis et al., 1996; and Tsintikidis et al., 1999).

In TIR based rainfall estimation, rainfall rates are inferred from cloud top surfaces. The underlying physical assumption is that relatively cold clouds are associated with thick and high clouds that tend to produce high rainfall rates. (Haile et al., 2010) described the limitation of these approaches: (i) different vertical profiles of clouds that result in different rainfall rates can have the same cloud top temperature, and (ii) TIR based approaches assume that rain occurs when the cloud top temperature is less than a selected threshold, e.g. (Griffith et al., 1978; Arkin 1979; Arkin and Meisner, 1987). As a result, the use of a constant temperature threshold introduces errors to the rainfall estimation procedure. (Todd et al., 1995) suggested the use of a TIR threshold that varies with geographic location and terrain elevation.

MW based approaches are based on the concept that observed radiation in the microwave frequencies is affected by atmospheric hydrometeors such as cloud and precipitation droplets that cause augmentation of radiation due to emission and attenuation of radiation due to absorption and scattering. As such, MW sensors respond primarily to precipitation-size hydrometeors in the cloud profile and therefore information from MW channels is much more direct as compared to information from TIR channels. However, we note that in MW approaches rainfall at the land surface cannot be retrieved directly. Currently, MW sensors are mounted only on low-altitude orbiting satellites and therefore the observations are snapshots that are available once or twice a day. Such observation frequency makes it difficult to capture the temporal dynamics of clouds.

The need to improve the performance of TIR and MW based rainfall retrieval approaches resulted in the development of combined approaches that benefit from

the strengths of both data sources. Such algorithms combine and benefit from TIR images at high temporal resolution and MW images that, compared to TIR, carry more direct information about cloud and rainfall characteristics. Examples of such approaches are PERSIANN (Hsu et al., 1997; Sorooshian, et al., 2000; Hong et al., 2005), NRLgeo (Turk and Miller, 2005), TRMM 3B42 (Huffman et al., 2007). As stated by (Haile et al., 2010), most of the rain products by these approaches are available at spatial resolutions $\geq 0.25°$ and temporal resolutions ≥ 1 day which is coarser than what is typically needed in hydrology and water resources. In addition, the validation of these products is still a topic of ongoing research.

Reviews by (Stephens and Kummerow, 2007; Levizzani et al., 2002; Barrett and Martin, 1991; Kidder and Vonder Haar, 1995; Petty, 1995) show that remote sensing based approaches of rainfall estimation have several limitation that lead to inaccurate rainfall estimates. In these reviews, the difficulty of validating remote sensing based estimates is noted since the use of rain gauge data is too poor in terms of resolution, reliability and in providing the spatial coverage of rainfall. Despite the poor performance, remote sensing has found applications in rainfall studies mainly since it provides a spatial coverage of rain producing clouds. Some applications of remote sensing include: rainfall detection to study the diurnal cycle of rainfall (Dai, 2001; Imaoka and Spencer, 2000), to monitor and characterize clouds that produce heavy rainfall (e.g. Feidas and Cartalis, 2001) and to analyze the scaling behaviour of rainfall (Gebremichael et al., 2008).

Nesbitt and Zipser (2003) noted that the limitations of diurnal cycle studies of rainfall revolve around (i) our inability to observe and quantify the true tropics wide diurnal cycle of rainfall amount and convective intensity, and (ii) the use of numerical model simulations that do not allow the true representation of the diurnal cycle. These limitations can be partly overcome by using remote sensing observations which are consistently available with spatially continuous coverage.

In this study, first we evaluate the use of remote sensing observations for rainfall estimation. Next, we present the diurnal cycle of rainfall using ground based observations and the diurnal cycle of convective activity using remote sensing observations in the Lake Tana basin, Ethiopia. Finally, the characteristics of a cloud that produced extreme rainfall intensity over Lake Tana are derived from MSG-2 observations. These characteristics include cloud area and volume index as well as temporal evolution of distance and direction of the centroid of a cloud mass from a rain gauge at the Gurer Island in Lake Tana.

4.2 Methods

4.2.1 Rainfall Diurnal Cycle

The diurnal cycle of rainfall is commonly analysed by estimating the frequency of rainfall occurrences that shows the percentage of rainy hours in a specific Local Standard Time (LST) of a selected time period, see (Haile et al., 2009; Gebremichael et al., 2007). The frequency of rainfall occurrences reads:

$$F_j = 100 \frac{\sum_{i=1}^{N} X_{ji}}{N} \tag{4.1}$$

where: F is the frequency of rainfall occurrences in specific LST (%), X is a flag for rainfall occurrence with $X = 0$ for non-rainy hours and $X = 1$ for rainy hours where a rainy hour in this study is defined based on the observation resolution of the rain gauges that is 0.2 mm. The index j indicates the LST under consideration while N is the number of days in the selected time period.

Remote sensing images also have found applications in diurnal cycle assessments of rainfall. For instance (Gebremichael et al., 2007) applied TRMM observations for detection of the rainfall cycle. However, TRMM provides intermittent observations of once or twice per day for a specific geographic location. Such introduces sampling error to the assessments of the diurnal cycle. For such assessment, MSG-2 is much more suitable since it observes a particular geographic location every 15 min. The large number of observations allow for statistical analysis. It is noted that TIR observations are proxy variables for the surface rainfall rate but by analysis of these observations we can infer patterns of convective activity, see (Ohsawa et al., 2001; Barros et al., 2004; Ba and Nicholson, 1998). In this study, the 10.8 μm brightness temperatures are analysed to study the temporal and spatial patterns of convective activity through a convective index (*CI*) that is defined as:

$$CI_h = 100 \left[\sum_{i=1}^{N} t_i \right] N^{-1} \tag{4.2}$$

where $t = 1$ for $T_l < T_{10.8} \leq T_u$, $t = 0$ for $T_{10.8} \leq T_l$ and $T_{10.8} > T_u$; N is the number of observations at a specific LST over a selected time period. In this study, the time period is from June 1 to August 25, 2007. We established indices that correspond to (i) $T_u < 210$ k, (ii) $T_u = 225$ k and $T_l = 210$ k and (iii) $T_u = 240$ k and $T_l = 225$ k to account for high, mid and low level clouds, respectively.

4.2.2 Convective Cloud Tracking

Through the MSG-2 satellite, we monitored a single cloud system that produced extreme rainfall in Lake Tana. Characteristics of the cloud that are monitored include the distance and the direction of the cloud centroid from the exact location of an automated rain recorder at Gurer Island in the lake, the cloud area and a cloud volume index. The cloud characteristics are derived following the procedure suggested by (Feidas and Cartalis, 2001); (Arnaud et al., 1992). The September 18, 2008 rain event is selected since the event produced extremely high intensity.

First, the centre of mass of the cloud is estimated. The coordinates of the centre of mass read:

$$X_c = \frac{\sum_{i=1}^{N} (Tb_{(TIR)i} + Tb_{(WV)i}) X_i}{\sum_{i=1}^{N} (Tb_{(TIR)i} + Tb_{(WV)i})},$$
$$Y_c = \frac{\sum_{i=1}^{N} (Tb_{(TIR)i} + Tb_{(WV)i}) Y_i}{\sum_{i=1}^{N} (Tb_{(TIR)i} + Tb_{(WV)i})} \tag{4.3}$$

where X_c and Y_c are the coordinates of the centre of mass of the cloud, respectively; i is a space index representing a pixel covered by a cloud; N is the number of cloudy pixels; Tb is the brightness temperature at the 6.2 and 10.8 μm channels that are the water vapour (WV) and thermal infrared (TIR) channels; and X_i and Y_i are the coordinates of the ith pixel covered by a cloud.

Next, the distance is measured from the centre of mass of the cloud to the location of the island rain gauge in Lake Tana. This is repeated for each time step. The direction is expressed in terms of an inclination, i.e. angle, which is measured from a Y-axis, with its origin at the rain gauge location, to the line that joins the rain gauge location and the centre of mass of the cloud. Positive direction indicates a clockwise angle from the Y-axis.

Cloud area is estimated as the number of pixels covered by a cloud multiplied by the size of a single pixel, i.e. 9 km^2 for MSG-2. Cloud area indicates the potential of the cloud to produce rainfall. Another indicator of the potential of a cloud to produce rainfall is the volume index (VI) which reads:

$$VI = \sum_{i=1}^{N} k_i (Tb_0 - Tb_i) \tag{4.4}$$

where k is the number of pixels with equal brightness temperature while the other terms are defined in previous paragraphs. Equation (4.4) is applied for both the TIR and WV channel and the average VI is used to measure the cloud potential to produce rainfall. We applied an arbitrarily chosen temperature threshold (Tb_0) of 240 K.

4.3 Results

4.3.1 Rainfall Estimation

The results in this section are based on the work by (Haile and Rientjes, 2007). Figures 4.1 and 4.2 illustrate that both daily minimum TIR brightness temperature (Tmin) and the Cold Cloud Duration (CCD) carry relevant information that

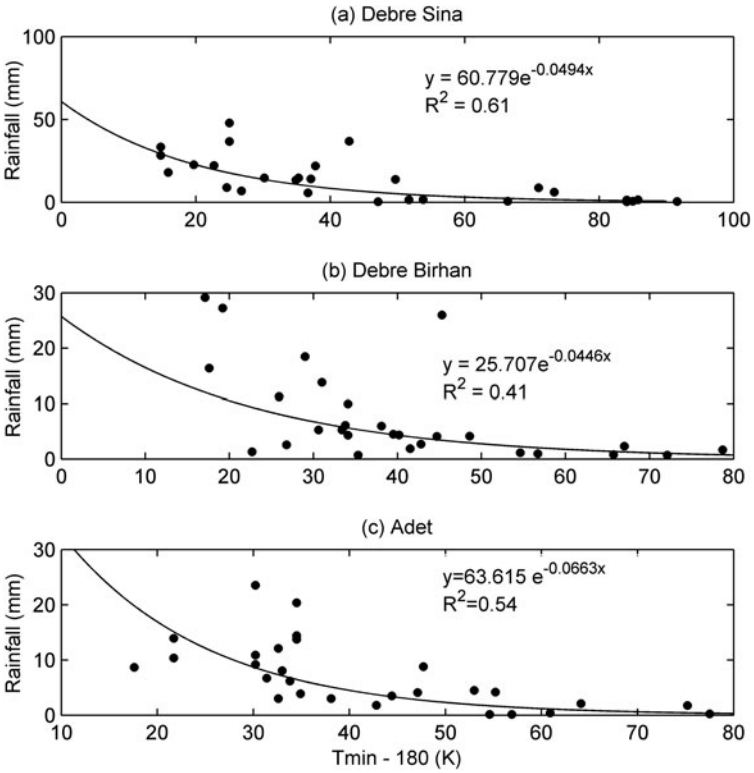

Fig. 4.1 Daily rainfall vs. daily minimum TIR brightness temperature observations for August, 2005. **a** For D/Sina meteorological station. **b** For D/Birhan meteorological station. **c** For Adet meteorological station

could be related to daily rainfall amounts. CCD is defined here as the duration over which a cloud top temperature of less than 260 K is observed. As it is shown in Fig. 4.1, a power law relationship between daily rainfall and daily minimum brightness temperature (Tmin) observations can be established. Although the coefficient of determination (i.e. R^2) is not very low, the relationship between the two variables is not very strong. Also the observed scattering indicates that the relation is non-unique since single brightness temperatures can be related to unequal daily rainfall depths. Nevertheless, the minimum brightness temperature is indicative towards daily rainfall amounts. For instance, for the considered stations, Tmin of less than 210 K is most likely associated to a rainfall amount higher than 10 mm while Tmin of greater than 230 K corresponds to a rainfall amount of lower than 5 mm.

The CCD is used as one of the indices for retrieval of daily rainfall amounts from images. A major limitation with the CCD is that rainfall amount is related mainly to the cloud duration. However, such assumptions could fail when convective clouds of high rainfall intensity occur over a short period of time. In addition and as observed

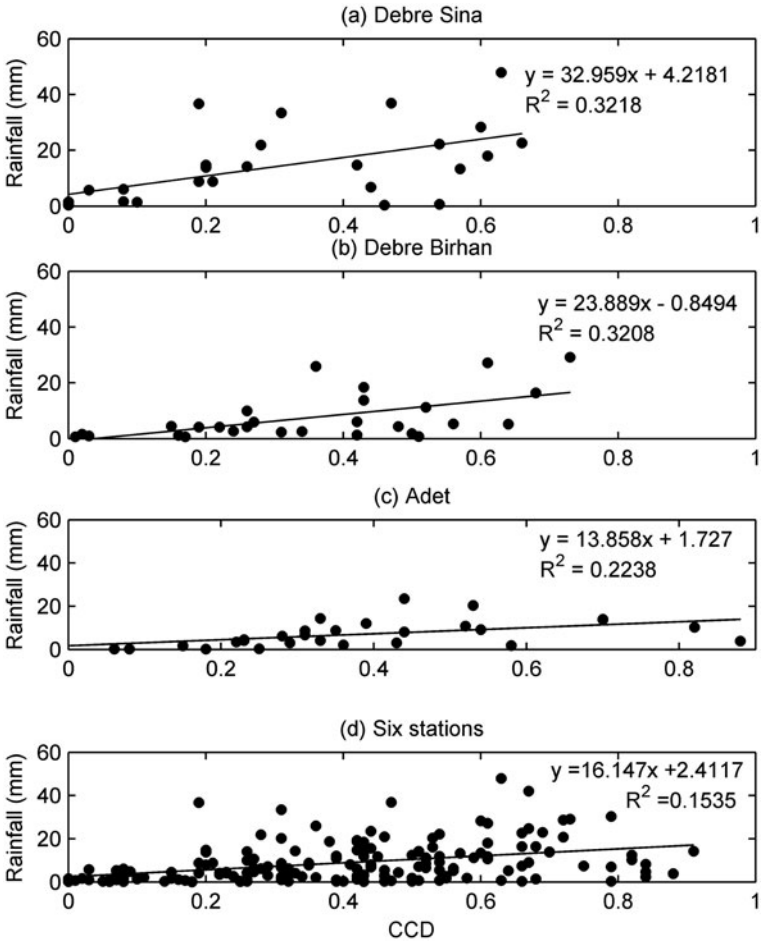

Fig. 4.2 Observed daily rainfall vs. daily CCD. **a** D/Sina. **b** D/Birhan. **c** Adet. **d** Six stations in the Upper Blue Nile basin

in similar studies, results from our approach are affected by the applied temperature threshold that varies with season and geographic position. In this study, the CCD values are computed based on a brightness temperature threshold of 260 K to detect rainfall from all types of clouds. It should however be understood that the threshold is affected by many factors and also changes over meso-scale spatial domains and season. However, several cloud indexing approaches use a constant threshold. Figure 4.2 shows that the R^2 value becomes lower when the relationship between observed daily rainfall and CCD values is established for combined observations from six stations as compared when the relationship is based on observations from a single station.

Table 4.1 Performance assessment of rainfall retrieval equations

Station	Equation	RE	RMSE	Rvar
	23.889 CCD-0.8494	0.66	6.82	0.32
	2×10^{24} $Tmin^{-10.104}$	0.55	7.00	0.16
D/Birhan	35.28+15.55 CCD-0.15 Tmin	0.64	6.59	0.37
	32.959 CCD+4.2181	0.56	10.74	0.32
	4×10^{27} $Tmin^{-11.398}$	0.48	10.25	0.54
D/Sina	72.82+16.81 CCD-0.3 Tmin	0.57	9.92	0.61
	13.858 CCD+1.727	0.53	5.28	0.22
	5×10^{35} $Tmin^{-14.962}$	0.53	5.58	0.71
Adet	54.72+3.42 CCD-0.22 Tmin	0.48	4.60	0.41
	16.147 CCD + 2.4117	0.71	9.59	0.02
	6×10^{22} $Tmin^{-9.4653}$	0.64	9.30	0.11
	44.56+6.95 CCD-0.18 Tmin	0.68	8.10	0.22
Six stations	30.64+12.66 CCD-0.19 Tmin+0.006 Elv	0.62	7.44	0.34

Table 4.1 shows the least square based regression equations and the performance indicators for rainfall estimation based on Tmin and/or CCD as explanatory variables. The performance of the applied regression equations is evaluated in terms of the Relative Error (RE), Root mean Square Error (RMSE) and the Relative variance (Rvar). RE is the ratio of the absolute error to the average of the observed data while Rvar is the ratio of the variance of the estimates to that of the observations. The optimal value for RE is zero and that for Rvar is one. As it is shown in Table 4.1 the errors of the estimates are relatively high and are about half of the averages of the observations. For the stations at D/Birhan and D/Sina, the Rvar and the RMSE become closer to the desired value when the estimates are based on both Tmin and CCD as compared to when only one of the two variables is considered. For the station at Adet, the RMSE becomes smaller when both Tmin and CCD are used, although the Rvar becomes closer to one when only Tmin is used.

Hydrological modeling requires spatial rainfall inputs that match the scale of the surface spatial units that make up the model domain. This requires formulation of a single relationship that is applicable to all elements that make up the land surface domain. Table 4.2 shows such equations for the Upper Blue Nile basin as based on rainfall observations for the month of August 2005 from six stations. The performance indicator values in Table 4.2 illustrate that formulation of a single best equation for the entire spatial domain requires additional explanatory variables for instance elevation (Elv.) in order to yield better performance.

4.3.2 Diurnal Cycle

The diurnal cycle of the convective index over Lake Tana and Gilgel Abbay watershed is shown in Fig. 4.3. Gilgel Abbay is the major contributor to the inflow of Lake

Table 4.2 Performance assessment of a single best rainfall retrieval equation

Equations	RE	RMSE	Rvar
44.56+6.95 CCD-0.18 Tmin			
D/Sina	0.68	6.79	0.22
D/Sina	0.62	12.17	0.18
Adet	0.52	4.8	0.39
30.64+12.66 CCD-0.19 Tmin+0.0056 Elv			
D/Birhan	0.68	6.69	0.36
D/Sina	0.54	10.68	0.27
Adet	0.55	5.07	0.69

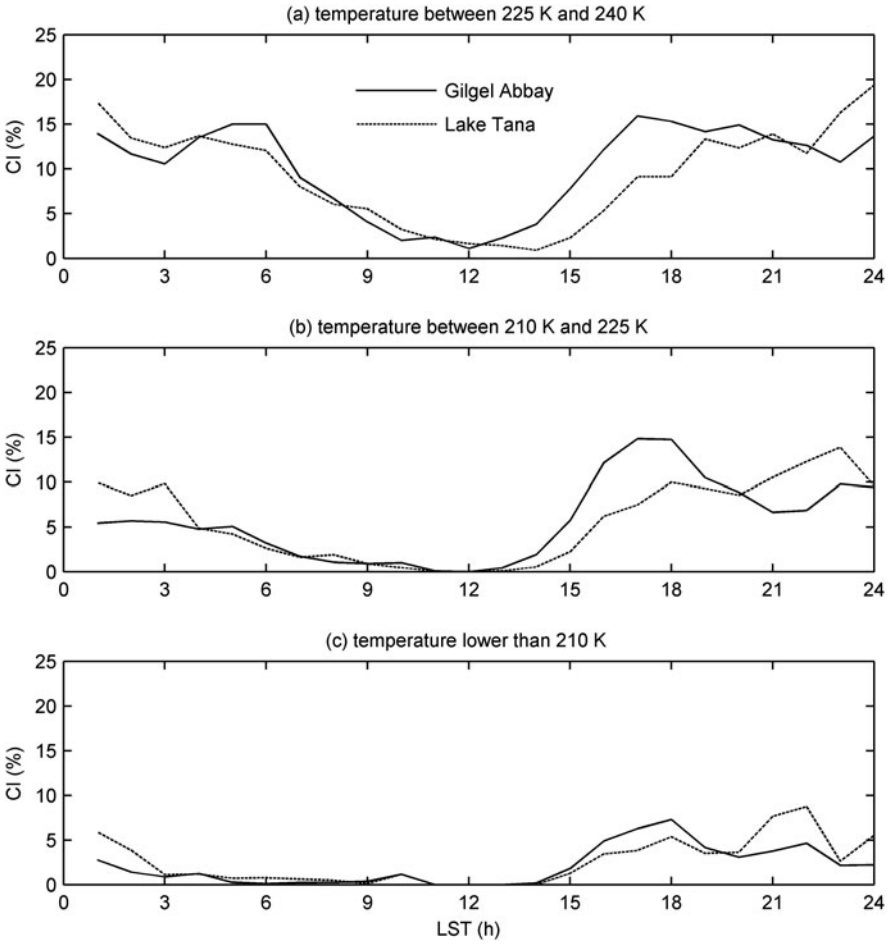

Fig. 4.3 Diurnal cycle of convective index for various temperature ranges of cloud top surface

Tana (see Wale et al., 2009). Figure 4.3a shows the diurnal cycle of CI for a temperature range between 225 and 240 K that represents low level clouds (LLC). The figure shows that the diurnal cycle of LLC over the land surface of Gilgel Abbay and over the lake area are somewhat different. The number indicates that cloud occurrence peaks at 1700 LST over the land surface and at 2300 LST over the lake. The figure shows that CI values in Gilgel Abbay vary within a small range between 1700 and 2400 LST. Such suggests that LLC probably has long duration in the watershed. Figure 4.3b shows the diurnal cycle of CI for a temperature range between 210 and 225 K which represent middle level clouds (MLC). The values of CI for MLC are much smaller than the values for HLC. The pattern of the CI of Lake Tana for MLC is similar to the pattern for LLC but over Gilgel Abbay, the diurnal cycle of CI for these two types of clouds is somewhat different.

The heaviest rain rates are commonly produced by high level clouds (HLC) that are thick. As such, understanding the diurnal cycle of HLC is important for many applications. Figure 4.3c shows the diurnal cycle of MLC occurrence in terms of CI for temperatures below 210 K. The figure shows that CI values are much smaller than those for MLC and LLC but the pattern is similar to that of the MLC except for small shifts in the time to peak. The CI of HLC peaks at 1800 LST and 2200 LST in Gilgel Abbay and Lake Tana respectively, suggesting the difference in the time of occurrence of heavy rainfall over the land and water surfaces.

4.3.3 Convective Cloud Tracking

In this section, we present the characteristic of the September 18, 2008 cloud that produced extreme rainfall intensity. We used the brightness temperature difference (BTD) which is defined as the difference between the brightness temperature at the 10.8 μm channel and the 6.2 μm channels ($T_{10.8} - T_{6.2}$). Figure 4.4 shows the distribution of the 1-min intensity (I_1) and BTD of the (extremely) high that was observed at the Island. The recorded rainfall intensity mostly ranges between 50 and 240 mm/h suggesting that the event had extremely heavy intensity throughout its duration with the highest intensities observed towards the end of the event. The BTD rapidly decreased towards zero when the rainfall commenced and became negative for most of the event duration. Then, the BTD immediately increased when the rainfall ceased.

The September 18 cloud was initiated between 1500 and 1600 LST at a distance of about 90 km from the island, see Figs. 4.5a and 4.6. The minimum Euclidean distance between the centre of mass of the cloud and the location of the rain gauge at the island is about 58 km which is observed at 1930 LST that is about 4 h after the initiation of the cloud. Note that the extreme rainfall at the island was observed between 1800 and 1937 LST. From 1930 onwards, the centroid of the cloud has moved away from the island. As such, although an extreme rainfall is observed at the Island, the center of mass of the cloud has never been over the Island. This suggests the heaviest rainfall presumably occurred at locations other than the Island.

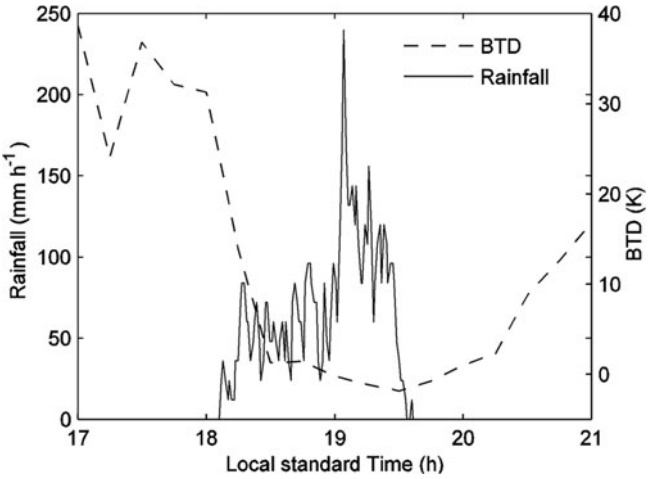

Fig. 4.4 The 1-min intensity and the brightness temperature difference (BTD) of the extreme rainfall that was observed on September 18, 2008

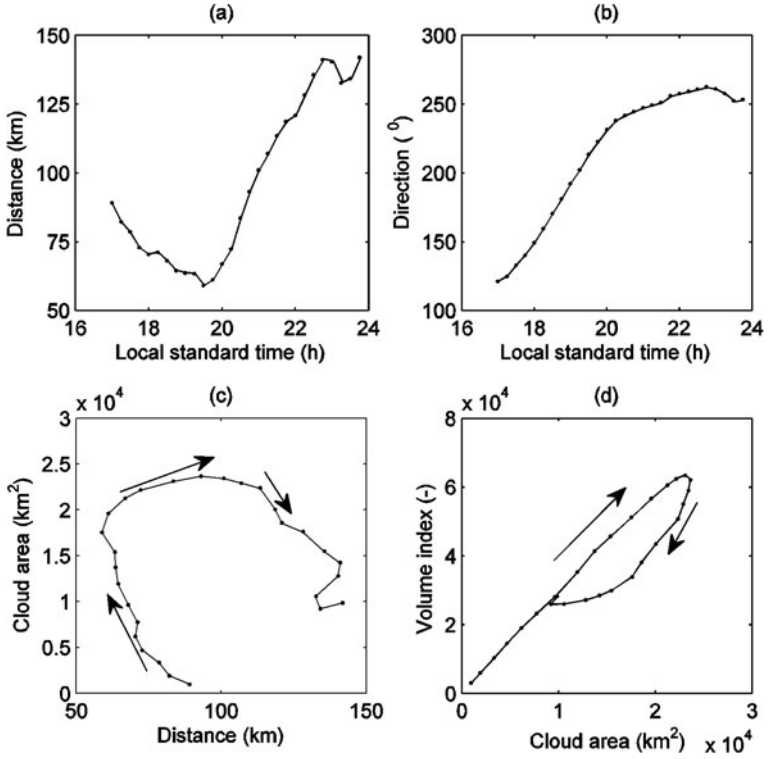

Fig. 4.5 Characteristics of the September 18, 2008 cloud that produced an extreme rainfall. Note: distance is measured from the island. The direction is expressed in terms of the angle that is measured from a *y*-axis, with its origin at the rain gauge location, to the line that joins the rain gauge location and the centre of mass of the cloud. Positive angle indicates clockwise direction

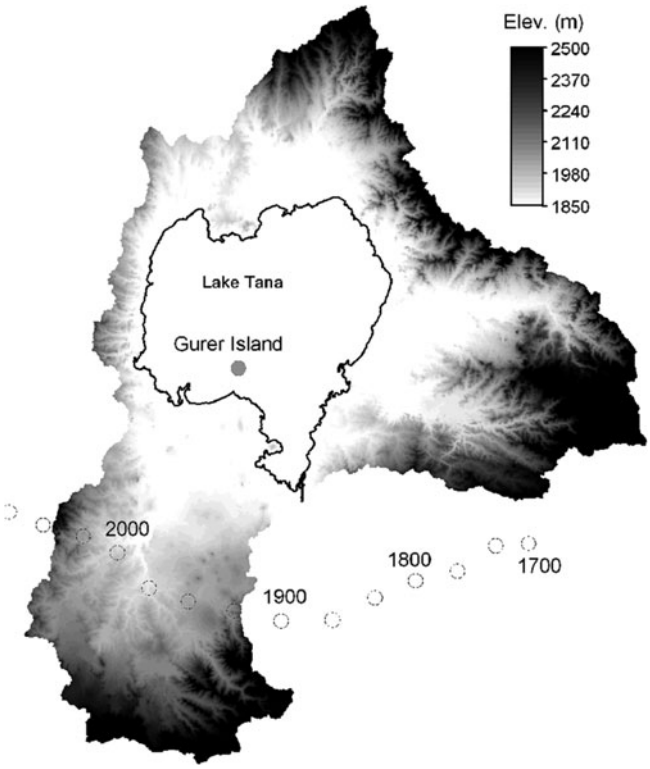

Fig. 4.6 The movement of the centroid of the cloud system with time. Note that: the centroids are represented by hollow circles and the local standard time for each centroid is also shown

Figure 4.5b shows the direction of the centre of mass of the cloud with respect to the rain gauge location at the island. Initially, the cloud centre was located south-east that is 120° of the island. The cloud centre was located south of the island during the time period, i.e. 18:00–19:37, at which the extreme rainfall was recorded. The cloud moved to south-east of the island afterwards. Both the distance and the direction of the cloud centroid show some trend suggesting that the timing and location of the September 18, 2008 extreme event could have been predicted when applying a technique of cloud tracking.

Figure 4.5c shows that the cloud area increases relatively rapidly as the cloud approaches the island. However, the area increases relatively slowly as the cloud moves away from the island and then it decreases afterwards. This suggests that although the cloud lost some rainwater at the island, its potential to produce heavy rainfall did not decrease immediately. We speculate that water vapour was extracted from the lake area to condense at higher altitude in the cloud to become cloud water. Such feedback causes the cloud to produce high rainfall rates.

The relation between cloud area and volume index is shown in Fig. 4.5d. The relation shows a loop suggesting that the volume increases with an increase in cloud

area during the cloud growth stage. The volume index decreased with a decrease in the cloud area during the cloud dissipation stage. The relation suggests that the volume index indicates the potential of a cloud to produce heavy rainfall however the index can have two values for an equal cloud area with the higher potential occurring during the growth stage. The largest value of the volume index occurred 15 min before the time to the largest value of the cloud area. This indicates that the potential of the cloud to produce heavy rainfall decreases although the cloud area increases towards the end of the growth stage. A similar observation is reported in (Feidas and Cartalis, 2001).

4.4 Discussion and Conclusion

We assessed the potential of remote sensing to characterise rainfall and clouds. Three topics are addressed: (i) rainfall estimation, (ii) rainfall detection for diurnal cycle analysis, and (iii) monitoring of extreme rainfall producing clouds.

For rainfall estimation, 2 indexes are derived from TIR observations: Cold Cloud Duration (CCD) and daily minimum temperature (Tmin) of cloud top surface. CCD indicates the duration over which a cloud is observed in a day while Tmin indicates the altitude of a cloud top surface. It is shown that CCD and daily rainfall are directly related but the R^2 values are found to be small and range between 0.15 and 0.32. The relationship between Tmin and daily rainfall are inversely related by a power law relation. The R^2 between Tmin and daily rainfall is relatively large and ranges between 0.42 and 0.61. The analysis indicates that daily rainfall exceeds 10 mm when Tmin of a cloud top surface is lower than 210 K while rainfall amounts of lower than 5 mm are generated by clouds with Tmin of higher than 230 K. Results indicate that formulation of a single best equation of rainfall estimation for the entire spatial domain requires additional explanatory variables, for instance, terrain elevation.

The diurnal cycle of rainfall over Lake Tana and over its major tributary (Gilgel Abbay watershed) is compared using a convective index (CI) that is established using TIR observations. The CI shows a clear difference between the pattern of the rainfall diurnal cycle over the lake and the land surface which suggests a difference in the rain generation mechanisms over the two surfaces. CI peaks in the night over the lake while it peaks in the afternoon over the land surface. The analysis also shows that low level clouds occur much more frequently in the study area than high level clouds.

Although TIR observations are the most commonly used remote sensing observations in rainfall estimation, we showed that brightness temperature difference (BTD) between TIR and WV channels provides additional information about surface rainfall intensities. It is shown that the BTD values rapidly decreases towards zero when the rainfall commences and becomes negative for most of the rain event duration. Then, the BTD value increases directly when the rainfall ceased. Such information is relevant for remote sensing based rainfall estimation.

We used TIR and WV brightness temperatures to monitor the characteristics of a cloud that produced extreme rainfall over Lake Tana. These characteristics are the distance and the direction of the cloud centre of mass with respect to the location of Gurer Island in Lake Tana. The analysis indicates that the heaviest rainfall from the cloud is generated at locations somewhat far from the Island although extreme rainfall is recorded at the Island.

The area covered by the cloud is monitored by using remote sensing observations. The analysis showed that the centre of mass of the cloud increased despite a loss of rain water when the cloud approaches Lake Tana. Such an increase in cloud area suggests the supply of moisture by Lake Tana that enhanced the water content of the cloud. The relationship between the volume index and the cloud area shows that although the potential of the cloud to produce rainfall decreases during the dissipation stage of the cloud, the cloud area still increases.

Overall, the results indicate the potential of remote sensing observations for rainfall studies. Remote sensing can be very helpful in estimating rainfall, assessing diurnal cycle and monitoring heavy rainfall producing clouds. Such potential of remote sensing observations is mainly because the observations are consistently available with spatial continuous coverage.

References

Arkin PA (1979) The relationship between fractional coverage of high cloud and rainfall accumulations during the GAGE over the B-scale array. Mon Wea Rev 107:1382–1387

Arkin PA, Meisner BN (1987) The relationship between large scale convective rainfall and cold cloud over the Western Hemisphere during 1982–1984. Mon Wea Rev 115:51–74

Arnaud Y, Desbois M, Maizi J (1992) Automatic tracking and characterization of African convective systems on Meteosat pictures. J Appl Meteor 31:443–453

Ba MB, Nicholson SE (1998) Analysis of convective activity and its relationship to the rainfall over the Rift Valley lakes of East Africa during 1983–1990 using meteosat infrared channel. J Appl Meteor 37:1250–1264

Barrett EC, Martin DW (1991) The use of satellite data in rainfall monitoring. Academic press, London, 340pp

Barros AP, Kim G, Williams E, Nesbitt SW (2004) Probing orographic controls in the Himalayas during the monsoon using satellite imagery. Nat Hazards Earth Syst Sci 4:29–51

Dai A (2001) Global precipitation and thunderstorm frequencies. Part II: diurnal variations. J Climate 14:1112–1128

Feidas H, Cartalis C (2001) Monitoring mesoscale convective cloud systems associated with heavy storms using meteosat imagery. J Appl Meteor 40:491–512

Gebremichael M, Krajewski WF, Over TM, Takayabu YN, Arkin P, Katayams M (2008) Scaling of tropical rainfall as observed by TRMM precipitation radar. Atmos Res 88:337–354

Gebremichael M, Vivoni ER, Watts CJ, Rodríguez JC (2007) Submesoscale spatiotemporal variability of North American monsoon rainfall over complex terrain. J Climate 20:1751–1773

Griffith CG, Woodley WL, Grube PG, Martin DW, Stout J, Sikdar DN (1978) Rain estimation from geosynchronous satellite imagery – visible and infrared studies. Mon Wea Rev 106:1153–1171

Haile AT, Rientjes THM (2007) Spatio-temporal rainfall mapping from space: setbacks and strengths. Proceedings of the 5th International symposium on Spatial Data Quality SDQ, Modelling qualities in space and time, ITC, Enschede, The Netherlands, 13–15 June, 2007, 9 p

Haile AT, Rientjes THM, Gieske A, Gebremichael M (2009) Rainfall variability over mountainous and adjacent lake areas: the case of Lake Tana basin at the source of the Blue Nile River. J App Meteorol Climatol 48:1696–1717

Haile AT, Rientjes TH, Gieske A, Gebremichael M (2010) Rainfall estimation at the source of the Blue Nile: a multispectral remote sensing approach. Int J Appl Earth Obs Geoinf JAG 12(Suppl. 1):S76–S82

Hong Y, Hsu KL, Sorooshian S, Gao X (2005) Improved representation of diurnal variability of rainfall retrieved from the tropical rainfall measurement mission MW imager adjusted precipitation estimation from remotely sensed information using artificial neural networks PERSIANN system. J Geophys Res 110:1–13

Hsu KL, Gao X, Sorooshian S, Gupta HV (1997) Precipitation estimation from remotely sensed imagery using an artificial neural network. J Appl Meteorol 36:1176–1190

Huffman GJ, Adler RF, Bolvin DT, Gu G, Nelkin EJ, Bowman KP, Hong Y, Stocker EF, Wolff DB (2007) The TRMM multisatellite precipitation analysis (TMPA): quasi-global, multiyear, combined-sensor precipitation estimates at fine scales. J Hydrometeor 8:38–55

Imaoka K, Spencer RW (2000) Diurnal variation of precipitation over the tropical oceans observed by TRMM/TMI combined with SSM/I. J Climate 13:4149–4158

Kidder SQ, Vonder Haar TH (1995) Satellite meteorology: an introduction. Academic Press, New York, 466pp

Levizzani V, Amorati R, Meneguzzo F (2002) A review of satellite-based rainfall estimation methods. European commission project MUSIC report EVK1-CT-2000-00058. 66pp. http://www.isac.cnr.it/~meteosat/pub.html

Lovejoy S, Austin GL (1979) The delineation of rain areas from visible and IR satellite data from GATE and mid-latitudes. Atmos Ocean 17:77–92

Nesbitt SW, Zipser EJ (2003) The diurnal cycle of rainfall and convective intensity according to the 3 years of TRMM measurements. J Climate 16:1456–1475

Ohsawa T, Ueda H, Hayashi T, Watanabe A, Matsumota J (2001) Diurnal variations of convective activity and rainfall in Tropical Asia. J Meteor Soc Japan 79:333–352

Petty GW (1995) The status of satellite-based rainfall estimation over land. Remote Sens Environ 51:125–137

Sorooshian S, Hsu KL, Gao X, Gupta HV, Imam B, Braithwaite D (2000) Evaluation of PERSIANN system satellite–based estimates of tropical rainfall. Bull Am Meteor Soc 81:2035–2046

Stephens GL, Kummerow CD (2007) The remote sensing of clouds and precipitation from space: a review. J Atmos Sci 64:3742–3765

Todd MC, Barrett EC, Beaumont MJ, Green JL (1995) Satellite identification of rain days over the upper Nile River basin using an optimum IR rain/no-rain threshold temperature model. J Appl Meteorol 34(12):2600–2611

Tsintikidis D, Georgakakos KP, Artan GA, Tsonis AA (1999) A feasibility study on mean areal rainfall estimation and hydrologic response in the Blue Nile region using METEOSAT images. J Hydrol 221:97–116

Tsonis AA, Triantafyllou GN, Georgaakakos KP (1996) Hydrological applications of satellite data 1. Rainfall estimation. J Geophys Res 101:26517–26525

Turk FJ, Miller SD (2005) Toward improving estimates of remotely-sensed precipitation with MODIS/AMSR-E blended data techniques. IEEE Trans Geosci Rem Sens 43:1059–1069

Wale A, Rientjes THM, Gieske ASM, Getachew HA (2009) Ungauged catchment contributions to Lake Tana's water balance. Hydrol Process 23(26):3682–3693